

This is an Open Access document downloaded from ORCA, Cardiff University's institutional repository: <https://orca.cardiff.ac.uk/id/eprint/136088/>

This is the author's version of a work that was submitted to / accepted for publication.

Citation for final published version:

Pan, Zhongmei, Wu, Jianzhong , Ding, Tao, Liu, Jian, Wang, Fei and Tong, Xiangqian 2020. Load flow calculation for droop-controlled islanded microgrids based on direct Newton-Raphson method with step size optimisation. IET Generation, Transmission and Distribution 14 (21) , pp. 4775-4787. 10.1049/iet-gtd.2019.1722

Publishers page: <http://dx.doi.org/10.1049/iet-gtd.2019.1722>

Please note:

Changes made as a result of publishing processes such as copy-editing, formatting and page numbers may not be reflected in this version. For the definitive version of this publication, please refer to the published source. You are advised to consult the publisher's version if you wish to cite this paper.

This version is being made available in accordance with publisher policies. See <http://orca.cf.ac.uk/policies.html> for usage policies. Copyright and moral rights for publications made available in ORCA are retained by the copyright holders.



# Load Flow Calculation for Droop-Controlled Islanded Microgrids Based on Direct Newton-Raphson Method with Step Size Optimization

Zhongmei Pan<sup>1\*</sup>, Jianzhong Wu<sup>2</sup>, Tao Ding<sup>3</sup>, Jian Liu<sup>1,4</sup>, Fei Wang<sup>1</sup>, Xiangqian Tong<sup>1</sup>

<sup>1</sup> School of Electrical Engineering, Xi'an University of Technology, Xi'an 710048, China

<sup>2</sup> School of Engineering, Cardiff University, Cardiff CF24 3AA, UK

<sup>3</sup> School of Electrical Engineering, Xi'an Jiaotong University, Xi'an 710049, China

<sup>4</sup> State Grid Shaanxi Electric Power Research Institute, Xi'an 710054, China

\*panpan@xaut.edu.cn

**Abstract:** Load flow calculation for droop-controlled islanded microgrids (IMGs) is different from that of transmission or distribution systems due to the absence of slack bus and the variation of frequency. Meanwhile considering the common three-phase imbalance condition in low-voltage systems, a load flow algorithm based on direct Newton-Raphson (NR) method with step size optimization for both three-phase balanced and unbalanced droop-controlled IMGs is proposed in this paper. First, the steady-state models for balanced and unbalanced droop-controlled IMGs are established based on their operational mechanisms. Then taking frequency as one of the unknowns, the nonlinear load flow equations are solved iteratively by NR method. Generally, iterative load flow algorithms are faced with challenges of convergence performance, especially for unbalanced systems. To tackle this problem, a step-size-optimization scheme is employed to improve the convergence performance for three-phase unbalanced IMGs. In each iteration, a multiplier is deduced from the sum of higher-order terms of Taylor expansion of the load flow equations. Then the step size is optimized by the multiplier which can help smooth the iterative process and obtain the solutions. The proposed method is performed on several balanced and unbalanced IMGs. Numerical results demonstrate the correctness and effectiveness of the proposed algorithm.

## Nomenclature

### A. Acronyms

DG	distributed generation
IMG	islanded microgrid
DFIG	doubly-fed induction generator
NR	Newton-Raphson
NRSSO	NR method with step size optimization
OM	optimal multiplier
LM	Levenberg-Marquart
ALM	adaptive Levenberg-Marquart

### B. Sets and Indices

$B$	Set of buses in a microgrid
$B_{Droop}/B_{PQ}/B_{PV}$	Set of droop/PQ/PV buses in a microgrid
$i, j$	Index of buses in a microgrid
$p, m$	Index of three phases
$k$	Index of iterations
$s$	Index of power flow equations

### C. Parameters

$Y_{ij}/\theta_{ij}$	amplitude/phase angle of the element in admittance matrix
$Y_{ik}^{mp}/\theta_{ik}^{mp}$	amplitude/phase angle of the element between phase $m$ at bus $i$ and phase $p$ at bus $k$ in admittance matrix
$P_{Li0}/Q_{Li0}$	rated active/reactive power for load at bus $i$
$P_{Li0}^m/Q_{Li0}^m$	rated active/reactive power for load of phase $m$ at bus $i$
$U_{i0}/\omega_{i0}$	rated voltage/frequency for load at bus $i$
$U_i^*/\omega^*$	voltage/frequency set point for droop-controlled DG at bus $i$
$m_{Pi}/n_{Qi}$	droop coefficients for droop-controlled DG at bus $i$
$k_{Pi}/k_{Qi}$	frequency regulation coefficients of active/reactive power for load at bus $i$
$\Delta P_i/\Delta Q_i$	active/reactive power mismatches at bus $i$
$\Delta P_i^m/\Delta Q_i^m$	active and reactive power mismatches in phase $m$ at bus $i$
$P_{IDGi}/Q_{IDGi}$	active/reactive power of intermittent DGs at bus $i$
$P_{IDGi}^m/Q_{IDGi}^m$	active/reactive power of phase $m$ of intermittent DGs at bus $i$
$A_{Pi}/A_{Qi}, B_{Pi}/B_{Qi}, C_{Pi}/C_{Qi}$	ZIP coefficients of active/reactive power for load at bus $i$
$A_{Pi}^m/A_{Qi}^m, B_{Pi}^m/B_{Qi}^m, C_{Pi}^m/C_{Qi}^m$	ZIP coefficients of active/reactive power for load of phase $m$ at bus $i$
$z_{ij}$	impedance of branch between bus $i$ and $j$
$z_{ij}^{abc}$	three-phase impedance matrix of branch between bus $i$ and $j$
$z_{ij}^{pm-n}$	impedance between phase $p$ and phase $m$ of the branch between bus $i$ and $j$

### D. Variables

$\omega$	angular frequency of the microgrid
$U_i/\delta_i, U_j/\delta_j$	amplitude/phase angle of voltage at bus $i, j$
$U_i^m/\delta_i^m, U_j^p/\delta_j^p$	amplitude/phase angle of voltage of phase $m$ at bus $i$ and of phase $p$ at bus $j$
$P_{Droopi}/Q_{Droopi}$	active/reactive power of droop-controlled DGs at bus $i$
$P_{Droopi}^\Sigma/Q_{Droopi}^\Sigma$	three-phase active/reactive power of droop-controlled DGs at bus $i$
$P_{Droopi}^m/Q_{Droopi}^m$	active/reactive power of $m$ -phase of droop-controlled DG at bus $i$ ;
$U_i^1$	positive sequence voltage amplitude at bus $i$ .

$P_{Li}/Q_{Li}$  active/reactive power for load at bus  $i$   
 $P_{L_i^m}/Q_{L_i^m}$  active/reactive power of phase  $m$  for load at bus  $i$

## 1. Introduction

As an effective way of utilization of clean energy, microgrid has been studied intensively in recent years. A microgrid can operate in grid-connected mode or islanded mode. When in islanded mode, dispatchable distributed generations (DGs) are generally responsible for the system frequency and voltage amplitude regulation. There are two control schemes for), i.e. centralized control scheme and decentralized droop control scheme [1-2]. Compared with the centralized control scheme which needs communication infrastructure and may suffer from single points of failure, the decentralized droop control scheme depends on local signals for load demand sharing and system regulation, thus has the merits of lower cost, higher reliability, and better expansibility [3-4].

Load flow calculation is the cornerstone for the planning and the operation of microgrids. Generally, in the planning and operation process, the load flow algorithm requires to be executed many times without human supervision, a guaranteed convergence with high computation efficiency is a desired feature [5].

Extensive studies have been carried out on load flow calculation for transmission and distribution systems [6-8]. However, conventional load flow models and algorithms are not applicable to droop-controlled IMGs because of their following features: 1) These IMGs are typically fed by several droop-controlled DG units of small capacity, thus no DG unit can serve as a slack bus, and the system frequency is not constant anymore; 2) The active and reactive power output as well as the voltage of the droop-controlled DGs are determined based on the droop characteristics, thus none of them can be pre-specified [3-4].

Therefore, several load flow algorithms have been addressed for droop-controlled IMGs. As two of the main load flow methods, backward/ forward sweep (BFS) method and Newton-Raphson (NR) method are tailored for droop-regulated microgrids [9-13]. In [9], the BFS method is expanded to two nested loops and voltage and frequency deviations are updated based on the droop functions. The algorithm proposed in [10], called forward-return-forward-backward sweep, combines BFS and a complementary inter-iteration method by using the point of common coupling as the reflection point. Although these two algorithms are derivative-free and inversion-free, they inherit the weakness of BFS method and become complicated for microgrids with multiple DGs or loops [9]. In [11], the load flow is calculated based on NR iterative procedure with a random bus selected as the slack bus. Therefore, an outer iteration loop is needed to force the active and reactive power flowing through the slack bus to zero, which results in more computation time. The methods proposed in [12] and [13] combine two additional equations of the total active power and reactive power of the whole system into the set of load flow equations and solve the problem by modified NR.

NR method may be faced with challenges of

convergence. Newton trust-region method and Levenberg-Marquart (LM) method, which is a type of trust region method, are employed widely to improve the convergence performance of iterative algorithm [14-16]. Newton trust-region algorithm is investigated in [17]. In [18] and [19], adaptive LM (ALM) method is implemented for load flow of droop-regulated IMGs.

However, load flow of unbalanced IMGs remains unaddressed in the above literature. In [20], a three-phase power flow model for droop-controlled IMGs is established and solved by Newton-trust region method to address the unbalanced conditions. However, in the dogleg step calculation of Newton-trust region method, the inverse of Hessian matrices is needed for calculating the steps. As the number of buses increases, the inversion step leads to high time cost and thus makes the algorithm inappropriate for online applications. The method proposed in [21] incorporates the conventional NR iterative method in a BFS sweep algorithm for load flow calculation for unbalanced loop-based microgrids, but more emphasis is laid on microgrids in grid-connected mode. Although the method is extended to islanded mode using the algorithm in [9], according to the conclusions in [21], the convergence performance needs to be improved further. In [22], a power flow analysis approach for balanced and unbalanced IMGs is proposed based on radial basis function neural networks by the input and output relationship of power-flow non-linear equation sets for the microgrids. However, it requires excessive simulation time to converge. In [23] a method based on particle swarm optimization with Gaussian mutation to minimize the mismatch of total active and reactive power, but the computation is time-consuming because of multiple iterations and optimizations.

To fill the gap in literature, a load flow algorithm based on direct NR method with step size optimization (NRSSO) for both balanced and unbalanced droop-controlled IMGs is proposed in this paper. The main contributions of this paper are as follows.

1) The load flow for balanced droop-controlled IMGs is solved by a direct NR method taking the angular frequency and voltages as unknown variables. No slack bus or additional equations are needed. And the convergence performance of the proposed algorithm is proved to be robust.

2) For unbalanced IMGs, load flow model is built and solved based on the direct NR method with step size optimization. In each iteration, the step size is scaled by an optimal multipliers (OM), which is derived based on the sum of high-order terms of Taylor expansion of power balance equations. Numerical results prove that the step size optimization technique is significant to guarantee the convergence performance of load flow in unbalanced IMGs.

The paper is organized as follows. The steady-state models of three-phase balanced and unbalanced droop-controlled IMGs are built respectively in Section II and Section III. In Section IV the problem formulation is presented. The proposed NRSSO method elaborated in Section V. Validation results are presented in Section VI. Conclusions are drawn in Section VII.

## 2. Modelling of balanced decentralized IMGs

### 2.1. Modelling of DGs

Generally, the output of non-dispatchable DGs such as wind turbines or photovoltaic units are determined by the input wind speed or sunlight intensity and the control methods. Therefore, the buses with these DG units integrated are represented as PQ buses or PV buses depending on the control mode of DG units: PQ buses in case of constant power factor control or PV buses in case of constant voltage control. Meanwhile the capacity of a non-dispatchable DG should be considered, e.g. for a DFIG-based wind turbine or a photovoltaic unit, the output power is generally constrained within D curve [24]. A PV bus with a DG of which the reactive power output arrives its limitation will be converted to a PQ bus.

Whereas for the dispatchable DGs in decentralized IMGs, e.g. micro-turbines and fuel cells, droop control strategy is employed to sustain voltage and frequency as well as balance the power supply and demand in IMGs. Usually these DGs are connected to the system through power electronic converters and output filters. At a steady-state operating point, the DG units combined with the converter and output filter, can be equivalent to an ideal controlled voltage source which is operated following droop control rules. Hence, the active and reactive output power of DG units vary with the system frequency and voltage magnitudes of their buses respectively as follows:

$$\begin{cases} \omega = \omega^* - m_{P_i} P_{\text{Droopi}} \\ U_i = U_i^* - n_{Q_i} Q_{\text{Droopi}} \end{cases} \quad (1)$$

where  $P_{\text{Droopi}}$  and  $Q_{\text{Droopi}}$  are the active and reactive output power of the droop-controlled DG at bus  $i$ , respectively;  $\omega$  is the angular frequency of the IMG;  $U_i$  is the voltage amplitude at bus  $i$ ;  $U_i^*$  and  $\omega^*$  are voltage and the angular frequency set point for the droop-controlled DG at bus  $i$ , respectively;  $m_{P_i}$  and  $n_{Q_i}$  are its droop coefficients, respectively.

### 2.2. Modelling of loads

The active and reactive power of loads may change with system frequency and bus voltages following their consumption characteristics. Owing to the small size and stochastic features of IMGs, the fluctuation of system frequency and bus voltages may be significant. Hence, the static frequency and voltage characteristics of loads are considered in modelling. Usually, the frequency characteristics of loads can be represented by frequency regulation coefficients. Similarly, the voltage characteristics can be represented as a static load model with the polynomial ZIP coefficients. Consequently, the load at bus  $i$  in an IMG is represented as:

$$\begin{cases} P_{L_i} = P_{L_{i0}} \left( A_{P_i} \left( \frac{U_i}{U_{i0}} \right)^2 + B_{P_i} \frac{U_i}{U_{i0}} + C_{P_i} \right) \cdot (1 + k_{P_i} (\omega - \omega_{i0})) \\ Q_{L_i} = Q_{L_{i0}} \left( A_{Q_i} \left( \frac{U_i}{U_{i0}} \right)^2 + B_{Q_i} \frac{U_i}{U_{i0}} + C_{Q_i} \right) \cdot (1 + k_{Q_i} (\omega - \omega_{i0})) \end{cases} \quad (2)$$

where  $P_{L_i}$ ,  $Q_{L_i}$ ,  $P_{L_{i0}}$  and  $Q_{L_{i0}}$  are the active power, reactive

power and their rated values of load at bus  $i$ , respectively;  $U_{i0}$  and  $\omega_{i0}$  are the rated voltage and frequency of load at bus  $i$ , respectively;  $k_{P_i}$  and  $k_{Q_i}$  are active and reactive power frequency regulation coefficients for load at bus  $i$ , respectively;  $A_{P_i}$ ,  $B_{P_i}$ ,  $C_{P_i}$  ( $A_{P_i} + B_{P_i} + C_{P_i} = 1$ ) and  $A_{Q_i}$ ,  $B_{Q_i}$ ,  $C_{Q_i}$  ( $A_{Q_i} + B_{Q_i} + C_{Q_i} = 1$ ) are the ZIP coefficients for active and reactive power for load at bus  $i$ , respectively;

### 2.3. Modelling of feeders

A distribution line is generally described by the PI model. The droop-controlled IMGs are usually developed from low-voltage distribution systems; thus, the parallel grounding capacitances of branches are generally negligible. Moreover, the dependency of the line inductance on the frequency is to be considered. Thus, a feeder between bus  $i$  and  $j$  can be represented as a series impedance  $z_{ij}(\omega)$ .

## 3. Modelling of unbalanced decentralized IMGs

### 3.1. Modelling of DGs

The buses of intermittent DGs can still be regarded as PQ buses or PV buses according to the control rules as well as the capacity limitation of the DGs in three-phase power flow calculation.

The droop-controlled DGs in three-phase unbalanced IMGs are modeled as follows:

$$\begin{cases} P_{\text{Droopi}}^\Sigma = \sum_{m=\{a,b,c\}} P_{\text{Droopi}}^m = \frac{\omega^* - \omega}{m_{P_i}} \\ Q_{\text{Droopi}}^\Sigma = \sum_{m=\{a,b,c\}} Q_{\text{Droopi}}^m = \frac{U_{i^*} - U_i^1}{n_{Q_i}} \end{cases} \quad (3)$$

where  $P_{\text{Droopi}}^\Sigma$  and  $Q_{\text{Droopi}}^\Sigma$  are three-phase total active and reactive power of droop-controlled DGs respectively;  $P_{\text{Droopi}}^m$  and  $Q_{\text{Droopi}}^m$  are their active power and reactive power of phase  $m$ ;  $U_i^1$  are the positive sequence voltage amplitude at bus  $i$ , which can be expressed by the three phase voltage  $U_i^m$  at bus  $i$  as follows:

$$U_i^1 = \frac{U_i^a + \alpha U_i^b + \alpha^2 U_i^c}{3}, \alpha = e^{j120^\circ} \quad (4)$$

Note that an energy storage system, the output power can be negative in state of charging. Moreover, if the output power of a DG or the SoC of an energy storage system in power flow results exceeds its limit, the bus of the DG should convert into a PQ bus. In addition, in this paper only the typical droop control rule in (1) and (3) is chosen for illustration, and the droop coefficients of three phases are set to be the same. However, the proposed algorithm can be adapted easily for other droop control rules, e.g.  $P$ - $V$ / $Q$ - $\omega$  and  $P$ - $V$ - $\omega$ / $Q$ - $V$ - $\omega$  rules, by replacing (1) or (3) with the respective formulae.

### 3.2. Modelling of loads

The ZIP combined three-phase unbalanced load model is employed in the load flow calculation. Considering its static voltage and frequency characteristics of load of phase  $m$  at bus  $i$ , its active power and reactive power can be expressed respectively as follows:

$$\begin{cases} P_{Li}^m = P_{Li0}^m \left( A_{Pi}^m \left( \frac{U_i^m}{U_{Li0}} \right)^2 + B_{Pi}^m \frac{U_i^m}{U_{Li0}} + C_{Pi}^m \right) \cdot (1 + k_{Pi}^m (\omega - \omega_{L0})) \\ Q_{Li}^m = Q_{Li0}^m \left( A_{Qi}^m \left( \frac{U_i^m}{U_{Li0}} \right)^2 + B_{Qi}^m \frac{U_i^m}{U_{Li0}} + C_{Qi}^m \right) \cdot (1 + k_{Qi}^m (\omega - \omega_{L0})) \end{cases} \quad (5)$$

where  $P_{Li}^m$ ,  $Q_{Li}^m$  and  $P_{Li0}^m$ ,  $Q_{Li0}^m$  are the active power, reactive power and their rated values of load of phase  $m$  respectively;  $A_{Pi}^m$ ,  $B_{Pi}^m$ ,  $C_{Pi}^m$  and  $A_{Qi}^m$ ,  $B_{Qi}^m$ ,  $C_{Qi}^m$  are the ZIP coefficients of the active and reactive load power of phase  $m$ , respectively.

### 3.3. Modelling of feeders

In three-phase unbalanced low-voltage IMGs, the equivalent circuits of branches can be calculated by the Carson's equations and Kron's reduction. Considering its dependence on frequency, the feeder between bus  $i$  and  $j$  can be expressed by a three-phase impedance matrix  $z_{ij}^{abc}$  as follows [1,16]:

$$z_{ij}^{abc}(\omega) = \begin{bmatrix} z_{ij}^{aa-n}(\omega) & z_{ij}^{ab-n}(\omega) & z_{ij}^{ac-n}(\omega) \\ z_{ij}^{ba-n}(\omega) & z_{ij}^{bb-n}(\omega) & z_{ij}^{bc-n}(\omega) \\ z_{ij}^{ca-n}(\omega) & z_{ij}^{cb-n}(\omega) & z_{ij}^{cc-n}(\omega) \end{bmatrix} \quad (6)$$

where  $z_{ij}^{pm-n}$  ( $p, m \in \{a, b, c\}$ ) is the impedance between phase  $p$  and phase  $m$  of the branch between bus  $i$  and  $j$  considering the effect of neutral line.

## 4. Load flow problem formulation

### 4.1. Problem formulation for balanced IMGs

Based on the operational features, the voltage and output power of droop-controlled DGs as well as the system frequency are all unknowns in the load flow model of IMGs. The buses to which droop-controlled DGs are connected are called droop buses in this paper. Therefore, there are three types of buses in the load flow model for droop-controlled IMGs: PQ buses, PV buses and droop buses.

Denote the set of PQ, PV and droop buses in an IMG as  $B$ , and  $B_{PQ}$ ,  $B_{PV}$  and  $B_{Droop}$  respectively. The load flow equations for the IMG can be formulated as follows. For any bus  $i \in B$ , there are two power balance equations:

$$\begin{cases} \Delta P_i = P_{Droopi} + P_{IDGi} - P_{Li} - U_i \sum_{j \in B} U_j Y_{ij} \cos(\theta_{ij} + \delta_j - \delta_i) = 0 \\ \Delta Q_i = Q_{Droopi} + Q_{IDGi} - Q_{Li} + U_i \sum_{j \in B} U_j Y_{ij} \sin(\theta_{ij} + \delta_j - \delta_i) = 0 \end{cases} \quad (7)$$

where  $\Delta P_i$  and  $\Delta Q_i$  are the active and reactive power mismatches at bus  $i$  respectively;  $P_{IDGi}$  and  $Q_{IDGi}$  are the active and reactive power of intermittent DGs such as wind-based DGs and photovoltaic systems integrated at bus  $i$  respectively;  $P_{Droopi}$ ,  $Q_{Droopi}$  are set zero for  $i \in B_{PQ}$  or  $i \in B_{PV}$ . The load power  $P_{Li}$ ,  $Q_{Li}$  can be calculated by (2) and respectively;  $Y_{ij}$  and  $\theta_{ij}$  are the amplitude and phase angle of the element in admittance matrix  $Y$ , respectively;  $U_j$  is the voltage magnitude at bus  $j$ ;  $\delta_i$  and  $\delta_j$  are the phase angles of voltage at bus  $i$  and  $j$ , respectively.

Similar to traditional load flow calculation, for each PQ bus, both voltage magnitude and angle are unknowns;

and for each PV bus, there is one unknown variable of angle and the balance equation of reactive power is not considered at the iteration stage of NR method. Whereas for each droop bus, both voltage magnitude and angle are variables. Meanwhile the angular frequency  $\omega$  is introduced as an unknown by the droop control rules. Consequently, for an IMG with  $N$  buses and  $N_{PV}$  PV buses, there are  $2 \times N - N_{PV}$  power balance equations in the load flow model. With an arbitrary bus selected as reference bus, i.e. its angle is set as zero, the number of the unknowns is  $2 \times N - N_{PV}$ .

Consequently, the power flow equations for an IMG can be expressed as follows:

$$\begin{cases} \Delta P(\delta, U, \omega) = 0 \\ \Delta Q(\delta, U, \omega) = 0 \end{cases} \quad (8)$$

where  $\Delta P$  and  $\Delta Q$  are the  $N$ -dimensional and  $N - N_{PV}$ -dimensional column vectors of active and reactive power mismatches in (7) respectively, i.e.  $\Delta P = [\{\Delta P_i\}, i \in B]^T$  and  $\Delta Q = [\{\Delta Q_i\}, i \in B \cap i \notin B_{PV}]^T$ ;  $\delta$ ,  $U$  and  $\omega$  are the  $(N-1)$ -dimensional,  $(N - N_{PV})$ -dimensional and one-dimensional column vectors of variables of voltage phase angle, amplitude and the system angular frequency respectively.

For the convenience of illustration, denote  $f$  as the  $(2 \times N - N_{PV})$ -dimensional column vector of mismatches of active power and reactive power in (8), i.e.  $f = [\Delta P \ \Delta Q]^T$ , and  $x$  as the  $(2 \times N - N_{PV})$ -dimensional column vector of variables, i.e.  $x = [\delta \ U \ \omega]^T$ . Then the power flow equations in (8) can be represented as:

$$f(x) = 0 \quad (9)$$

### 4.2. Problem formulation for unbalanced IMGs

For an unbalanced decentralized IMG, the three-phase active and reactive load flow equations can be expressed as:

$$\begin{cases} \Delta P_i^m = P_{Droopi}^m + P_{IDGi}^m - P_{Li}^m - P_i^m = 0 \\ \Delta Q_i^m = Q_{Droopi}^m + Q_{IDGi}^m - Q_{Li}^m - Q_i^m = 0 \end{cases} \quad m = \{a, b, c\} \quad (10)$$

$$\begin{cases} P_i^m = U_i^m \sum_{j \in B} \sum_{p=\{a,b,c\}} U_j^p Y_{ij}^{mp} \cos(\theta_{ij}^{mp} + \delta_j^p - \delta_i^m) \\ Q_i^m = -U_i^m \sum_{j \in B} \sum_{p=\{a,b,c\}} U_j^p Y_{ij}^{mp} \sin(\theta_{ij}^{mp} + \delta_j^p - \delta_i^m) \end{cases} \quad (11)$$

where  $\Delta P_i^m$  and  $\Delta Q_i^m$  are the active and reactive power mismatches in phase  $m$  at bus  $i$  respectively;  $Y_{ik}^{mp}$  and  $\theta_{ik}^{mp}$  are the amplitude and phase angle of the element between phase  $m$  at bus  $i$  and phase  $p$  at bus  $k$  in admittance matrix, respectively;  $U_i^m$ ,  $\delta_i^m$  and  $U_j^p$ ,  $\delta_j^p$  are the voltage amplitude and phase angle in phase  $m$  at bus  $i$  and phase  $p$  at bus  $j$  respectively;  $P_{IDGi}^m$  and  $Q_{IDGi}^m$  are the active and reactive power of intermittent DGs in phase  $m$  at bus  $i$ , respectively. For  $i \in B_{PQ}$  or  $i \in B_{PV}$ ,  $P_{Droopi}^m$  and  $Q_{Droopi}^m$  are set zero.

In addition to the six power balance equations in (10), for each  $i \in B_{Droop}$ , the total three-phase output active and reactive power of DG follows droop control rules in (3) simultaneously. Generally, the three-phase voltages at a droop bus are symmetrical, whereas the power of each phase is not necessarily equal due to the asymmetry of system structure and parameters. Therefore, the voltage and power at a droop bus must satisfy the following 6 equations:

$$\begin{cases} P_{\text{Droopi}}^a + P_{\text{Droopi}}^b + P_{\text{Droopi}}^c - \frac{\omega_0 - \omega}{m_{\text{Pi}}} = 0 \\ Q_{\text{Droopi}}^a + Q_{\text{Droopi}}^b + Q_{\text{Droopi}}^c - \frac{U_{i0} - U_i^1}{n_{\text{Qi}}} = 0 \end{cases} \quad i \in B_{\text{Droop}} \quad (12)$$

$$\begin{cases} U_i^a - U_i^b = U_i^a - U_i^c = 0 \\ \delta_i^a - \delta_i^b - \left(\frac{2\pi}{3}\right) = \delta_i^a - \delta_i^c + \left(\frac{2\pi}{3}\right) = 0 \end{cases} \quad i \in B_{\text{Droop}} \quad (13)$$

Consequently, for each droop bus  $i \in B_{\text{Droop}}$ , there are 12 equations of 12 unknown variables: three-phase voltage amplitude, phase angle and three-phase output power. To simplify the calculation, for any  $i \in B_{\text{Droop}}$ , 6 of the 12 unknowns are eliminated based on the symmetry of its nodal voltage, which are  $U_i^b$ ,  $U_i^c$ ,  $\delta_i^b$ ,  $\delta_i^c$ ,  $P_{\text{Droopi}}^b$  and  $Q_{\text{Droopi}}^b$ . Thus only 6 unknown variables of  $U_i^a$ ,  $\theta_i^a$ ,  $P_{\text{Droopi}}^a$ ,  $P_{\text{Droopi}}^c$ ,  $Q_{\text{Droopi}}^a$  and  $Q_{\text{Droopi}}^c$  are to be calculated.

Then the mismatches of active and reactive power in phase  $m$  for each droop bus  $i \in B_{\text{Droop}}$  can be expressed as:

$$\begin{cases} \Delta P_i^a = P_{\text{Droopi}}^a + P_{\text{IDGi}}^a - P_{\text{Li}}^a - P_i^a = 0 \\ \Delta P_i^b = P_{\text{Droopi}}^b + P_{\text{IDGi}}^b - P_{\text{Li}}^b - P_i^b = 0 \\ \Delta P_i^c = \frac{\omega_0 - \omega}{m_{\text{p}}} - P_{\text{Droopi}}^c - P_{\text{Droopi}}^b + P_{\text{IDGi}}^c - P_{\text{Li}}^c - P_i^c = 0 \\ \Delta Q_i^a = Q_{\text{Droopi}}^a + Q_{\text{IDGi}}^a - Q_{\text{Li}}^a - Q_i^a = 0 \\ \Delta Q_i^b = Q_{\text{Droopi}}^b + Q_{\text{IDGi}}^b - Q_{\text{Li}}^b - Q_i^b = 0 \\ \Delta Q_i^c = \frac{U_{\text{Droopi}0}^a - U_{\text{Droopi}}^a}{n_{\text{Q}}} - Q_{\text{Droopi}}^c - Q_{\text{Droopi}}^b + Q_{\text{IDGi}}^c - Q_{\text{Li}}^c - Q_i^c = 0 \end{cases} \quad (14)$$

According to the above analysis, for any  $i \in B_{\text{Droop}}$ , the number of unknowns is in line with the number of equations. The equations of PQ buses and PV buses are the same as those in traditional load flow calculation. Meanwhile, an arbitrary one of the angles of nodal voltage is chosen as a reference phase angle and the system frequency is treated as an unknown variable. Consequently, the number of unknowns is consistent with the number of equations.

Thus, the three-phase power flow equations can be expressed as follows:

$$\begin{cases} \Delta \mathbf{P}^{abc}(\boldsymbol{\delta}^{abc}, \mathbf{U}^{abc}, \omega, \mathbf{P}_{\text{Droop}}^{ab}, \mathbf{Q}_{\text{Droop}}^{ab}) = 0 \\ \Delta \mathbf{Q}^{abc}(\boldsymbol{\delta}^{abc}, \mathbf{U}^{abc}, \omega, \mathbf{P}_{\text{Droop}}^{ab}, \mathbf{Q}_{\text{Droop}}^{ab}) = 0 \end{cases} \quad (15)$$

where  $\Delta \mathbf{P}^{abc}$  and  $\Delta \mathbf{Q}^{abc}$  are the column vectors of active and reactive power mismatches in (11) or (14) respectively, i.e.  $\Delta \mathbf{P}^{abc} = [\Delta P_i^m, i \in B, m \in \{a, b, c\}]^T$  and  $\Delta \mathbf{Q}^{abc} = [\Delta Q_i^m, i \in B \cap i \notin B_{\text{PV}}, m \in \{a, b, c\}]^T$ , and their dimensions are  $3 \times N$  and  $3 \times (N - N_{\text{PV}})$  respectively;  $\boldsymbol{\delta}^{abc}$  is the phase angle column vector of three-phase voltage at both PQ buses and PV buses as well as of phase  $a$  at droop buses with dimension of  $3 \times N - 2 \times N_{\text{Droop}} - 1$ ;  $\mathbf{U}^{abc}$  is the amplitude column vector of three-phase voltage at PQ buses and of phase  $a$  at droop buses with dimension of  $3 \times (N - N_{\text{PV}}) - 2 \times N_{\text{Droop}}$ .  $\mathbf{P}_{\text{Droop}}^{ab}$  and  $\mathbf{Q}_{\text{Droop}}^{ab}$  are the  $(2 \times N_{\text{Droop}})$ -dimensional column vectors composed of the active and reactive power output of droop-controlled DGs of phase  $a$  and  $b$  at droop buses, respectively.

Denote the column vector of mismatches of three-phase active power and reactive power in (15) as  $\mathbf{F}$ , i.e.  $\mathbf{F} = [\Delta \mathbf{P}^{abc} \Delta \mathbf{Q}^{abc}]^T$ , and denote the column vector of unknowns in (15) as  $\mathbf{X}$ , i.e.  $\mathbf{X} = [\boldsymbol{\delta}^{abc} \mathbf{U}^{abc} \omega \mathbf{P}_{\text{Droop}}^{ab} \mathbf{Q}_{\text{Droop}}^{ab}]^T$ . Then the power flow equations in (15) can be represented as:

$$\mathbf{F}(\mathbf{X}) = 0 \quad (16)$$

## 5. NR algorithm with step size optimization

### 5.1. Direct NR algorithm for IMGs

NR algorithm is one of the most common iterative methods for solving nonlinear equations. In this paper, it is applied to the load flow equations in (9) and (16). Based on the principle of NR method, after the initial values are given, the unknown variables can be obtained by solving the step and updating the unknown variables iteratively until the stop criterion is met [12].

For the equations of a balanced IMG in (9), the load flow equations can be expressed approximately by the linear part of its Taylor series expansion as follows:

$$\mathbf{f}(\mathbf{x} + \Delta \mathbf{x}) \approx \mathbf{f}(\mathbf{x}) + \mathbf{J} \cdot \Delta \mathbf{x} = \begin{bmatrix} \Delta \mathbf{P} \\ \Delta \mathbf{Q} \end{bmatrix} + \mathbf{J} \cdot \begin{bmatrix} \Delta \boldsymbol{\delta} \\ \Delta \mathbf{U} \\ \Delta \omega \end{bmatrix} = 0 \quad (17)$$

where  $\mathbf{J}$  is the Jacobian matrix, the elements of which are the partial derivatives of  $\mathbf{f} = [\Delta \mathbf{P} \Delta \mathbf{Q}]^T$  with respect to  $\mathbf{x} = [\boldsymbol{\delta} \mathbf{U} \omega]^T$ . Therefore,  $\mathbf{J}$  can be express by 6 partitioned matrices:

$$\mathbf{J} = \frac{\partial \mathbf{f}}{\partial \mathbf{x}} = \begin{bmatrix} \mathbf{H} & \mathbf{N} & \mathbf{E} \\ \mathbf{M} & \mathbf{L} & \mathbf{F} \end{bmatrix} = \begin{bmatrix} \frac{\partial \Delta \mathbf{P}}{\partial \boldsymbol{\delta}} & \frac{\partial \Delta \mathbf{P}}{\partial \mathbf{U}} & \frac{\partial \Delta \mathbf{P}}{\partial \omega} \\ \frac{\partial \Delta \mathbf{Q}}{\partial \boldsymbol{\delta}} & \frac{\partial \Delta \mathbf{Q}}{\partial \mathbf{U}} & \frac{\partial \Delta \mathbf{Q}}{\partial \omega} \end{bmatrix} \quad (18)$$

where  $\mathbf{H}$ ,  $\mathbf{N}$ ,  $\mathbf{M}$ ,  $\mathbf{L}$ ,  $\mathbf{E}$  and  $\mathbf{F}$  are partitioned matrices which can be deduced from (8).

In the  $k$ -th ( $k \geq 0$ ) iteration of the conventional NR method,  $\mathbf{x}^{(k)} = [\boldsymbol{\delta}^{(k)} \mathbf{U}^{(k)} \omega^{(k)}]^T$  is given ( $k=0$ ) or obtained from last iteration ( $k > 0$ );  $\mathbf{f}^{(k)}(\mathbf{x}^{(k)}) = [\Delta \mathbf{P}^{(k)}(\mathbf{x}^{(k)}) \Delta \mathbf{Q}^{(k)}(\mathbf{x}^{(k)})]^T$  and  $\mathbf{J}^{(k)}$  can be calculated from (7) and (17) respectively. Then the step size  $\Delta \mathbf{x}^{(k)}$  can be determined by:

$$\Delta \mathbf{x}^{(k)} = \begin{bmatrix} \Delta \boldsymbol{\delta}^{(k)} \\ \Delta \mathbf{U}^{(k)} \\ \Delta \omega^{(k)} \end{bmatrix} = -(\mathbf{J}^{(k)})^{-1} \mathbf{f}^{(k)}(\mathbf{x}^{(k)}) = -(\mathbf{J}^{(k)})^{-1} \begin{bmatrix} \Delta \mathbf{P}^{(k)} \\ \Delta \mathbf{Q}^{(k)} \end{bmatrix} \quad (19)$$

After the step  $\Delta \mathbf{x}^{(k)}$  is obtained,  $\mathbf{x}$  is updated:

$$\mathbf{x}^{(k+1)} = \mathbf{x}^{(k)} + \Delta \mathbf{x}^{(k)} \quad (20)$$

The iteration of (19)-(20) are carried out repeatedly until the stop criterion is met, i.e.  $\|\mathbf{f}\|_{\infty} < \varepsilon$  ( $\varepsilon$  is the tolerance) or the iteration number reaches its maximum.

Similarly, for an unbalanced IMG, perform the following iteration until  $\|\mathbf{F}\|_{\infty} < \varepsilon$  or the iteration number reaches its maximum. In the  $k$ -th ( $k \geq 0$ ) iteration, we have:

$$\begin{cases} \Delta \mathbf{X}^{(k)} = -(\mathbf{J}^{(k)})^{-1} \cdot \mathbf{F}^{(k)}(\mathbf{X}^{(k)}) \\ \mathbf{X}^{(k+1)} = \mathbf{X}^{(k)} + \Delta \mathbf{X}^{(k)} \end{cases} \quad (21)$$

$$\mathbf{J}^{abc} = \frac{\partial \mathbf{F}}{\partial \mathbf{X}} = \begin{bmatrix} \frac{\partial \Delta \mathbf{P}^{abc}}{\partial \boldsymbol{\delta}^{abc}} & \frac{\partial \Delta \mathbf{P}^{abc}}{\partial \mathbf{U}^{abc}} & \frac{\partial \Delta \mathbf{P}^{abc}}{\partial \omega} & \frac{\partial \Delta \mathbf{P}^{abc}}{\partial \mathbf{P}_{\text{Droop}}^{ab}} & \frac{\partial \Delta \mathbf{P}^{abc}}{\partial \mathbf{Q}_{\text{Droop}}^{ab}} \\ \frac{\partial \Delta \mathbf{Q}^{abc}}{\partial \boldsymbol{\delta}^{abc}} & \frac{\partial \Delta \mathbf{Q}^{abc}}{\partial \mathbf{U}^{abc}} & \frac{\partial \Delta \mathbf{Q}^{abc}}{\partial \omega} & \frac{\partial \Delta \mathbf{Q}^{abc}}{\partial \mathbf{P}_{\text{Droop}}^{ab}} & \frac{\partial \Delta \mathbf{Q}^{abc}}{\partial \mathbf{Q}_{\text{Droop}}^{ab}} \end{bmatrix} \quad (22)$$

## 5.2. NRSSO algorithm

The traditional NR algorithm stated above is proved to be able to converge well for balanced IMGs in practice, however, its performance is not so satisfied in cases of unbalanced IMGs. Hence, the NRSSO method is proposed for better convergence via optimizing the step sizes in the iteration of NR load flow for unbalanced IMGs. The NRSSO method integrates mathematical programming to the standard NR algorithm. In NRSSO, OMs are determined by solving the minimum problem of the objective function consisting of the load flow equations. In each iteration, the update vector scaled by OM are used to update the results.

The load flow method with OMs was first conceived in rectangular coordinates [25] and extended into polar coordinates [26] for ill-conditioned systems. The performance of the methods in polar coordinates is proved to be more effective than in rectangular coordinates in [27] due to the good linearization of load flow equations in polar form. Note that in the aforementioned works, only the information of the second-order term from the Taylor expansion is used in computation of OMs. The calculation is more accurate if more information can be exploited by taking higher-order terms into account. Hence, a NR method with OMs using the sum of high-order terms of the Taylor expansion in polar coordinates is adopted in this paper. The procedures of the NRSSO algorithm are as follows.

For clarity and considering that the traditional NR algorithm for unbalanced IMGs are more prone to diverge, only power flow equations of unbalanced ones are selected for illustration below. Note that it is suitable for both balanced and unbalanced IMGs.

Notice that in (21) only the linear terms of the Taylor expansion of load flow equations are preserved. This may introduce errors in the iteration, resulting in poor convergence performance. Thus, in the NRSSO method for the unbalanced IMGs, the step is scaled by an OM, i.e. not  $\Delta\mathbf{X}^{(k)}$  but  $\mu^{(k)} \cdot \Delta\mathbf{X}^{(k)}$  is employed for iteration as follows:

$$\mathbf{X}^{(k+1)} = \mathbf{X}^{(k)} + \mu^{(k)} \cdot \Delta\mathbf{X}^{(k)} \quad (23)$$

where  $\mu^{(k)}$  is the OM in the  $k$ -th iteration.

The OMs can be deduced by exploring more information in the Taylor series expansion of  $\mathbf{F}(\mathbf{X})$  as follows.

First, an optimization model is built with the objective function  $\mathfrak{R}(\mathbf{X})$  defined as:

$$\mathfrak{R}(\mathbf{X}) = \frac{1}{2} \|\mathbf{F}(\mathbf{X})\|^2 = \frac{1}{2} \mathbf{F}(\mathbf{X})^\top \cdot \mathbf{F}(\mathbf{X}) \quad (24)$$

Obviously, when  $\mathbf{F}(\mathbf{X}) = 0$ ,  $\mathfrak{R}(\mathbf{X})$  gets its minimum 0.

Then, the Taylor series expansion of  $\mathbf{F}(\mathbf{X})$  is carried out as:

$$\mathbf{F}(\mathbf{X} + \Delta\mathbf{X}) = \mathbf{F}(\mathbf{X}) + \mathbf{J}^{abc} \cdot \Delta\mathbf{X} + \Phi(\Delta\mathbf{X}) \quad (25)$$

where  $\Phi(\Delta\mathbf{X})$  is the sum of all of the nonlinear terms in the Taylor expansion of  $\mathbf{F}(\mathbf{X})$ , i.e.

$$\Phi(\Delta\mathbf{X}) = \frac{\mathbf{F}''(\mathbf{X})}{2!} (\Delta\mathbf{X})^2 + \frac{\mathbf{F}^{(3)}(\mathbf{X})}{3!} (\Delta\mathbf{X})^3 + \dots \quad (26)$$

And when  $\mu \cdot \Delta\mathbf{X}$  is employed, we have:

$$\mathbf{F}(\mathbf{X} + \mu\Delta\mathbf{X}) = \mathbf{F}(\mathbf{X}) + \mathbf{J}^{abc} \cdot \mu\Delta\mathbf{X} + \Phi(\mu\Delta\mathbf{X}) \quad (27)$$

In the  $k$ -th iteration, substitute (27) into (24), perform

Taylor series expansion of  $\mathfrak{R}(\mathbf{X})$  at  $\mathbf{X}^{(k)}$  as follows:

$$\begin{aligned} \mathfrak{R}(\mathbf{X}^{(k)} + \mu^{(k)} \Delta\mathbf{X}^{(k)}) &= \frac{1}{2} \|\mathbf{F}(\mathbf{X}^{(k)} + \mu^{(k)} \Delta\mathbf{X}^{(k)})\|^2 \\ &= \frac{1}{2} \|\mathbf{F}(\mathbf{X}^{(k)}) + \mu^{(k)} \mathbf{J}^{abc(k)} \Delta\mathbf{X}^{(k)} + \Phi(\mu^{(k)} \Delta\mathbf{X}^{(k)})\|^2 \end{aligned} \quad (28)$$

If  $\|\Delta\mathbf{X}^{(k)}\|$  approaches 0 or the OM  $\mu^{(k)}$  approaches 1, we have

$$\Phi(\mu^{(k)} \Delta\mathbf{X}^{(k)}) \approx (\mu^{(k)})^2 \Phi(\Delta\mathbf{X}^{(k)}) \quad (29)$$

Substitute (29) into (28):

$$\begin{aligned} \mathfrak{R}(\mathbf{X}^{(k)} + \mu^{(k)} \Delta\mathbf{X}^{(k)}) &= \frac{1}{2} \|\mathbf{F}(\mathbf{X}^{(k)}) + \mu^{(k)} \mathbf{J}^{abc(k)} \Delta\mathbf{X}^{(k)} + (\mu^{(k)})^2 \Phi(\Delta\mathbf{X}^{(k)})\|^2 \end{aligned} \quad (30)$$

Notice that in the  $k$ -th iteration standard  $\Delta\mathbf{X}^{(k)}$  can be obtained from (21) beforehand, and by substituting it into (30), we have:

$$\begin{aligned} \mathfrak{R}(\mathbf{X}^{(k)} + \mu^{(k)} \Delta\mathbf{X}^{(k)}) &= \frac{1}{2} \|\mathbf{F}(\mathbf{X}^{(k)}) - \mu^{(k)} \mathbf{F}^{(k)}(\mathbf{X}^{(k)}) + (\mu^{(k)})^2 \Phi^{(k)}(\Delta\mathbf{X}^{(k)})\|^2 \end{aligned} \quad (31)$$

For load flow equations  $\mathbf{F}(\mathbf{X})$  in polar coordinates,  $\Phi(\Delta\mathbf{X})$  has infinite nonlinear terms and cannot be obtained by accumulation term by term. It is calculated as follows. In the  $k$ -th iteration, after  $\Delta\mathbf{X}^{(k)}$  is obtained from (21), substitute it into (25), and the nonlinear total term can be calculated by:

$$\Phi^{(k)}(\Delta\mathbf{X}^{(k)}) = \mathbf{F}(\mathbf{X}^{(k)} + \Delta\mathbf{X}^{(k)}) \quad (32)$$

Denote the total number of equations in (16) as  $n_{eq}$ , i.e.  $\mathbf{F}(\mathbf{X}) = [F_1(\mathbf{X}) \cdots F_i(\mathbf{X}) \cdots F_{n_{eq}}(\mathbf{X})]^\top$ . Let:

$$a_i^{(k)} = F_i(\mathbf{X}^{(k)}) \quad (33)$$

$$c_i^{(k)} = F_i(\mathbf{X}^{(k)} + \Delta\mathbf{X}^{(k)}) \quad (34)$$

And substitute (33)-(34) into (31):

$$\mathfrak{R}(\mathbf{X}^{(k)} + \mu^{(k)} \Delta\mathbf{X}^{(k)}) = \frac{1}{2} \sum_{s=1}^{n_{eq}} (a_s^{(k)} - \mu^{(k)} a_s^{(k)} + (\mu^{(k)})^2 c_s^{(k)})^2 \quad (35)$$

According to Fermat's theorem, i.e. interior extremum theorem, when the partial derivative of  $\mathfrak{R}(\mathbf{X})$  with respect to  $\mu$  is zero,  $\mathfrak{R}(\mathbf{X} + \mu \cdot \Delta\mathbf{X})$  reaches its minimum. As can be seen from (28), when  $\mathfrak{R}(\mathbf{X} + \mu \cdot \Delta\mathbf{X})$  is minimum,  $\mathbf{F}(\mathbf{X})$  is nearest to zero. Therefore, the obtained OMs  $\mu$  can ensure a more accurate correction toward the final solution of load flow equations. The partial derivative of  $\mathfrak{R}(\mathbf{X})$  with respect to  $\mu$  at the  $k$ -th iteration is calculated from (35), and we have:

$$\frac{\partial \mathfrak{R}}{\partial \mu^{(k)}} = g_3 (\mu^{(k)})^3 + g_2 (\mu^{(k)})^2 + g_1 \mu^{(k)} + g_0 = 0 \quad (36)$$

$$g_3 = 2 \sum_{s=1}^{n_{eq}} (c_s^{(k)})^2; g_2 = -3 \sum_{s=1}^{n_{eq}} a_s^{(k)} c_s^{(k)}; \quad (37)$$

$$g_1 = 2 \sum_{s=1}^{n_{eq}} ((a_s^{(k)})^2 + 2a_s^{(k)} c_s^{(k)}); g_0 = -\sum_{s=1}^{n_{eq}} (a_s^{(k)})^2$$

The cubic equation of (36) can be solved by root-seeking methods such as Cardan's formula or NR method, etc. Generally, there are three real roots or one real root and a pair of conjugate complex roots for the cubic equation. When there is only one real root, the real root is selected as the OM of the  $k$ -th iteration  $\mu^{(k)}$ ; otherwise, the one corresponding to

the minimum value of the function  $F$  is selected to be  $\mu^{(k)}$ .

To summarize the procedures of the proposed direct NR method, a flowchart for the main program and a flow chart of the subprogram of NRSSO are presented in Fig. 1(a) and (b) respectively. The corresponding steps are outlined as follows.

*Step 1.* Set  $k=0$ . Initialize the unknown variables  $\mathbf{x}^{(k)}$  in (9) or  $\mathbf{X}^{(k)}$  in (16)

*Step 2.* Calculate the power mismatches and the Jacobian matrix.

*Step 3.* Calculate the update vector  $\Delta\mathbf{x}^{(k)}$  based on (19) or  $\Delta\mathbf{X}^{(k)}$  based on (21), and update  $\mathbf{x}^{(k)}$  or  $\mathbf{X}^{(k)}$ .

*Step 4.* Repeat Steps 2 and 3 and stop when the convergence criterion is met. Otherwise go next step and start the subprogram of NRSSO after the iteration number reaches its limit.

*Step 5.* Set  $k=0$ . Initialize the unknowns  $\mathbf{x}^{(k)}$  or  $\mathbf{X}^{(k)}$ .

*Step 6.* Calculate the update vector  $\Delta\mathbf{x}^{(k)}$  based on (19) or  $\Delta\mathbf{X}^{(k)}$  based on (21), and get  $\mathbf{x}^{(k)}+\Delta\mathbf{x}^{(k)}$  or  $\mathbf{X}^{(k)}+\Delta\mathbf{X}^{(k)}$  for the calculation of  $a_i^{(k)}$  and  $c_i^{(k)}$  using (33) and (34).

*Step 7.* Calculate the coefficients  $g_0^{(k)}$ ,  $g_1^{(k)}$ ,  $g_2^{(k)}$  and  $g_3^{(k)}$  of the cubic equation in (36).

*Step 8.* Solve the cubic equation and obtain  $\mu^{(k)}$ .

*Step 9.* Update  $\mathbf{x}^{(k)}$  or  $\mathbf{X}^{(k)}$  using the update vector scaled by  $\mu^{(k)}$ .

*Step 10.* Repeat Step 2~ Step 5 until the convergence criterion is met or the iteration number reaches its limit.

## 6. Algorithm validation

The proposed model and algorithm are tested on several balanced and unbalanced IMGs. To validate the proposed NR and NRSSO method, the results are compared with the traditional LM and ALM method to illustrate the convergence of the algorithm.

### 6.1. Test of direct NR method on Balanced IMGs

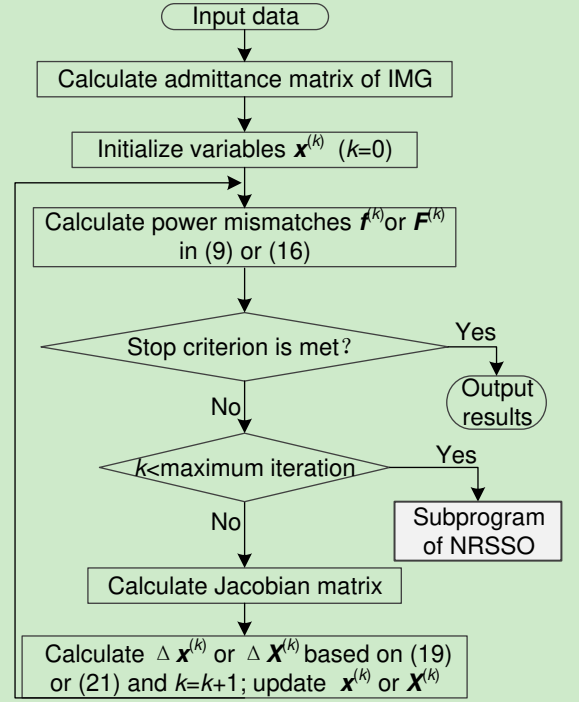
**Case 1.** The proposed algorithm for balanced IMGs is validated on an IMG system modified from the IEEE 33-bus distribution system. The single-line diagram and its parameters can be found in [28]. Four dispatchable and droop-controlled DGs are connected at 18, 22, 25 and 33, respectively. The detailed parameters (in p.u.,  $S_B=1\text{MVA}$ ) of the droop-controlled DGs are given in Table 1. In the ZIP load model, same coefficients are considered for simplicity, i.e. for each bus  $i$ , we have  $A_{Pi}=0.3$ ,  $B_{Pi}=0.3$ ,  $C_{Pi}=0.4$ ,  $A_{Qi}=0.3$ ,  $B_{Qi}=0.3$ ,  $C_{Qi}=0.4$ ,  $k_{Pi}=2$  and  $k_{Qi}=-2$ .

Considering that  $R/X$  ratio and feeder loading can affect the power flow convergence, to show the robustness of the proposed method, two scenarios are tested:

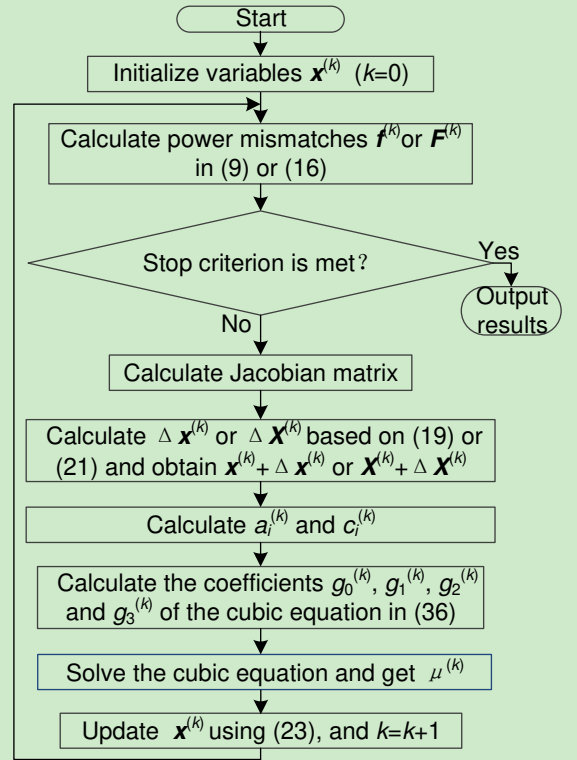
Scenario I. The IMG of original parameter settings;

Scenario II. The microgrid with higher  $R/X$  ratio and heavier loading, where  $R/X$  ratio is quadrupled through  $R$  increased by 50% and  $X$  reduced to 50%, and loads are increased by 50% of the original.

The proposed direct NR algorithm is applied to power load calculation of the IMG. According to the above parameters, there are 4 droop buses, 29 PQ buses and no PV buses in this 33-bus IMG. For each bus, we have two power balance equations, so  $\mathbf{f}=[\Delta P_1, \dots, \Delta P_{33}; \Delta Q_1, \dots, \Delta Q_{33}]^T$ . Take the voltage angle of an arbitrary bus say  $\delta_l$  as the reference



(a) Flow chart for the main program



(b) Flow chart for the subprogram of NRSSO

Fig. 1. Flowchart of the proposed flow calculation method.

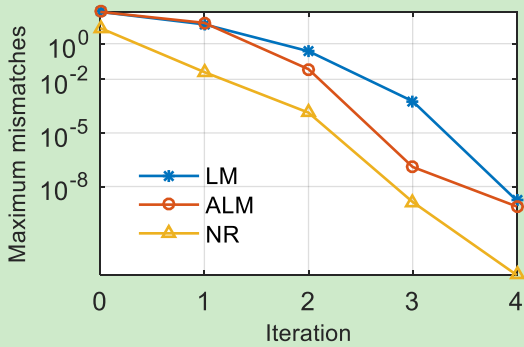
Table 1 Droop parameters for DGs in 33-bus IMG (p.u.)

Bus No.	Rated capacity	$U_{i*}$	$\omega_*$	$m_P$	$n_Q$
18	0.8	1.05	1.004	0.01333	0.300
22	1.0	1.05	1.004	0.01000	0.200
25	2.5	1.05	1.004	0.00400	0.080
33	3.0	1.05	1.004	0.00333	0.067

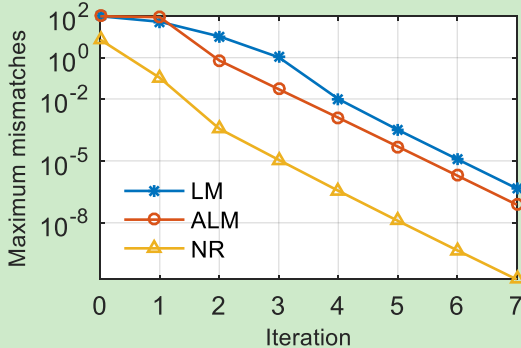
angle. The unknowns in load flow calculation are voltage angle  $\delta_i$  ( $i=2, 3 \dots 33$ ), magnitude  $U_i$  ( $i=1, 2 \dots 33$ ) and the angular frequency  $\omega$ , thus in (9)  $\mathbf{x}=[\delta_2, \dots, \delta_{33}; U_1, \dots, U_{33}; \omega]^T$ . Consequently, both  $\mathbf{f}$  and  $\mathbf{x}$  are column vectors with dimension of  $66 \times 1$ . Then a  $66 \times 66$ -dimensional Jacobin matrix  $\mathbf{J}$  is composed of the partial derivatives of each element in  $\mathbf{f}$  with respect to each element in  $\mathbf{x}$  in each iteration. For initialization,  $U_i^{(0)}=1$  ( $i=1, 2 \dots 33$ ),  $\delta_i^{(0)}=0$  ( $i=2, 3 \dots 33$ ) and  $\omega^{(0)}=1$ . Then the iteration is performed until  $\|\mathbf{f}\|_\infty < \varepsilon$  ( $\varepsilon=10^{-5}$  p.u.).

To investigate the performance of the proposed method, load flow in the two scenarios are calculated by LM, ALM method and the direct NR method. The voltage and frequency (in p.u.) of the 33-bus IMG are given in Table 2. The convergence curves of maximum mismatches, i.e.  $\|\mathbf{f}\|_\infty$  (in p.u.) of the two scenarios are plotted in Fig. 2.

**Case 2.** The algorithm is tested further on an IMG modified from the IEEE 69-bus system with three droop-controlled DGs connected at 8, 12 and 61, respectively. The



(a) Scenario I



(b) Scenario II

Fig. 2. Maximum mismatches (p.u.) for 33-bus IMG

Table 2 Voltage and frequency of the 33-bus IMG (p.u.)

Bus No.	Voltage	Bus No.	Voltage	Bus No.	Voltage
1	0.9683 $\angle 0^\circ$	12	0.9553 $\angle -0.1079^\circ$	23	0.9696 $\angle -0.0074^\circ$
2	0.9683 $\angle 0^\circ$	13	0.9554 $\angle -0.1819^\circ$	24	0.9741 $\angle -0.0437^\circ$
3	0.9679 $\angle 0.0208^\circ$	14	0.9559 $\angle -0.2065^\circ$	25	0.9818 $\angle -0.0372^\circ$
4	0.9666 $\angle 0.0682^\circ$	15	0.9570 $\angle -0.2271^\circ$	26	0.9638 $\angle 0.2387^\circ$
5	0.9656 $\angle 0.1151^\circ$	16	0.9586 $\angle -0.2490^\circ$	27	0.9649 $\angle 0.2896^\circ$
6	0.9632 $\angle 0.2027^\circ$	17	0.9631 $\angle -0.2042^\circ$	28	0.9692 $\angle 0.5891^\circ$
7	0.9615 $\angle 0.0585^\circ$	18	0.9647 $\angle -0.1742^\circ$	29	0.9729 $\angle 0.8221^\circ$
8	0.9591 $\angle 0.0470^\circ$	19	0.9686 $\angle -0.0032^\circ$	30	0.9758 $\angle 0.9123^\circ$
9	0.9572 $\angle -0.0256^\circ$	20	0.9730 $\angle -0.0134^\circ$	31	0.9863 $\angle 1.0993^\circ$
10	0.9557 $\angle -0.0893^\circ$	21	0.9747 $\angle 0.0039^\circ$	32	0.9902 $\angle 1.1924^\circ$
11	0.9555 $\angle -0.0950^\circ$	22	0.9785 $\angle 0.0679^\circ$	33	0.9960 $\angle 1.3860^\circ$
$\omega$	1.0032				

single-line diagram and its parameters can be found in [29]. The droop parameters (in p.u.,  $S_B=1\text{MVA}$ ) of DGs are given in Table 3. The parameters in ZIP load model at all buses are set the same as those of the 33-bus IMG.

The proposed direct NR algorithm is applied to this IMG. There are 3 droop buses, 66 PQ buses and none PV buses in this 69-bus IMG, so  $\mathbf{f}=[\Delta P_1, \dots, \Delta P_{69}; \Delta Q_1, \dots, \Delta Q_{69}]^T$ . With  $\delta_l$  as the reference angle, the unknowns in the problem are voltage angle  $\delta_i$  ( $i=2, 3 \dots 69$ ), voltage magnitude  $U_i$  ( $i=1, 2 \dots 69$ ) and the angular frequency  $\omega$ , thus  $\mathbf{x}=[\delta_2, \dots, \delta_{69}; U_1, \dots, U_{69}; \omega]^T$ . Consequently, both  $\mathbf{f}$  and  $\mathbf{x}$  are column vectors with dimension of  $138 \times 1$ . Then a  $138 \times 138$ -dimensional Jacobin matrix  $\mathbf{J}$  is composed of the partial derivatives of each element in  $\mathbf{f}$  with respect to each element in  $\mathbf{x}$  in each iteration. For initialization,  $U_i^{(0)}=1$  ( $i=1, 2 \dots 69$ ),  $\delta_i^{(0)}=0$  ( $i=2, 3 \dots 69$ ) and  $\omega^{(0)}=1$ . Then the iteration is performed until  $\|\mathbf{f}\|_\infty < \varepsilon$  ( $\varepsilon=10^{-5}$  p.u.).

Load flow for the 69-bus IMG in the two above-mentioned scenarios as in the 33-bus IMG are calculated by LM, ALM method and the proposed NR method. The maximum mismatches, i.e.  $\|\mathbf{f}\|_\infty$  (in p.u.) curves of the two scenarios are plotted in Fig. 3.

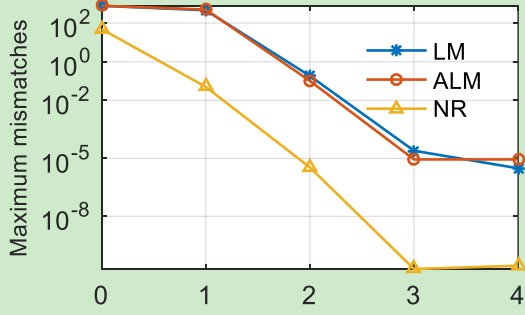
**Case 3.** The third case is an IMG modified from a 141-bus system. Six droop-controlled DGs are connected at 18, 25, 33, 74, 87 and 100, respectively. The single-line diagram and its parameters can be found in [30]. The detailed parameters (in p.u.,  $S_B=1\text{MVA}$ ) of droop-controlled DGs are given in Table 4. The parameters in ZIP load model at all buses are the same as those of the 33-bus IMG.

As can be seen there are 6 droop buses and 135 PQ buses in this 141-bus IMG, similarly,  $\mathbf{f}=[\Delta P_1, \dots, \Delta P_{141}; \Delta Q_1, \dots, \Delta Q_{141}]^T$ ,  $\mathbf{x}=[\delta_2, \dots, \delta_{141}; U_1, \dots, U_{141}; \omega]^T$ . And the Jacobin matrix  $\mathbf{J}$  consists of  $282 \times 282$  elements of the partial derivatives of  $\mathbf{f}$  with respect to  $\mathbf{x}$  in each iteration.

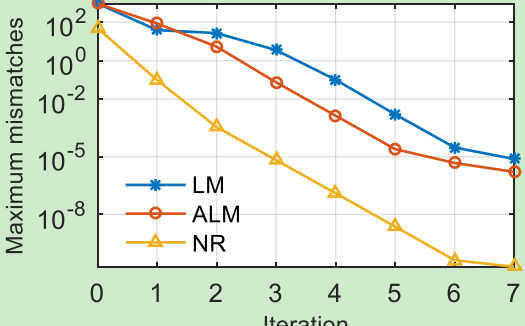
Load flow in the two scenarios of the 141-bus IMG are calculated by LM, ALM method and the proposed NR method. The curves of maximum mismatches, i.e.  $\|\mathbf{f}\|_\infty$  (in p.u.) of the two scenarios are plotted in Fig. 4

Table 3 Droop parameters for DGs in 69-bus IMG (p.u.)

Bus No.	Rated capacity	$U_i^*$	$\omega^*$	$m_P$	$n_Q$
8	3.0	1.03	1.004	0.0008	0.004
12	1.6	1.03	1.004	0.0010	0.010
61	3.2	1.03	1.004	0.0005	0.005

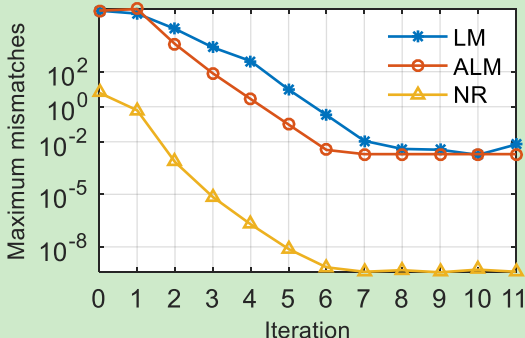


(a) Scenario I

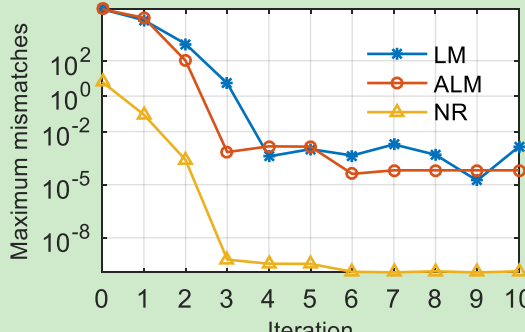


(b) Scenario II

Fig. 3. Maximum mismatches (p.u.) in the two scenarios for the 69-bus IMG



(a) Scenario I



(b) Scenario II

Fig. 4. Maximum mismatches (p.u.) for 141-bus IMG

Table 4 Droop parameters for DGs in 141-bus IMG (p.u.)

Bus No.	Rated capacity	$U_i^*$	$\omega^*$	$m_p$	$n_Q$
18	0.8	1.05	1.004	0.0133	0.030
25	1.0	1.05	1.004	0.0040	0.080
33	2.5	1.05	1.004	0.0333	0.067
74	3.0	1.05	1.004	0.0133	0.030
87	3.0	1.05	1.004	0.0100	0.200
100	0.8	1.05	1.004	0.0040	0.080

Table 6 Computation time (s) of the three methods for different IMGs in Scenario II.

Time	LM	ALM	NR
33-bus	0.0123	0.0116	0.0048
69-bus	0.0235	0.0215	0.0051
141-bus	NC*	NC*	0.0092

\*NC means "Not convergent"

As can be seen in Fig.2-Fig.4, when  $\varepsilon=10^{-5}$  p.u., the iteration number of the three method in Scenario I and Scenario II are given in Table 5. Further, the computation time for the three IMGs in Scenario II is given in Table 6.

The results of the three cases show that the proposed direct NR method for balanced IMG is effective, and so no optimization of step size is needed. The direct NR method converges in less iterations than the LM and ALM method specially for heavily loaded IMGs. Meanwhile, its execution time is much less than LM and ALM.

## 6.2. Test of NRSSO on Unbalanced IMGs

**Case 1.** The proposed model and algorithm are tested on an IMG modified from a 0.4kV 6-bus system. The single-line diagram of IMG is shown in Fig.5, with the switch at PCC point off. A fuel-cell-based DG and a micro-gas-turbine-based DG are droop-controlled, connected at Bus 1 and Bus 6 respectively. The parameters of the two DGs are given in Table 7. Assuming that the conductors of all branches are of the same type, and the three-phase self-impedance of per unit length are as follows:  $Z_{aa}=1.1980+j0.8820\Omega/\text{km}$ ,  $Z_{bb}=1.1997+j0.8833\Omega/\text{km}$ ,  $Z_{cc}=1.2015+j0.8846\Omega/\text{km}$ , and the mutual impedance of per unit length is supposed to be  $Z_{mm}=0.0100+j0.0735\Omega/\text{km}$ . Details of the system parameters are shown in Appendix 1 for table of the length of each branch and the three-phase load power. The ZIP coefficients and the static frequency coefficients of each bus and phase in the load model are set the same as in the balanced 33-bus IMG.

Table 7 The parameters of droop-controlled DGs in the 6-bus IMG (p.u.)

Bus No.	Rated capacity	$U^*$	$\omega^*$	$m_p$	$n_Q$
1	0.75	1.05	1.0	0.0040	0.08
6	0.75	1.05	1.0	0.0040	0.08

Table 5 Number of iterations of the three methods for different IMGs.

Iterations	Scenario I			Scenario II		
	LM	ALM	NR	LM	ALM	NR
33-bus	4	3	3	7	6	4
69-bus	4	4	2	7	7	3
141-bus	NC*	NC*	3	NC*	NC*	3

\*NC means "Not convergent"

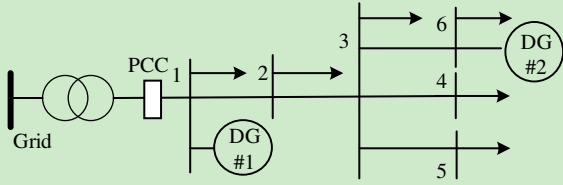


Fig. 5. The single-line diagram of 6-bus IMG

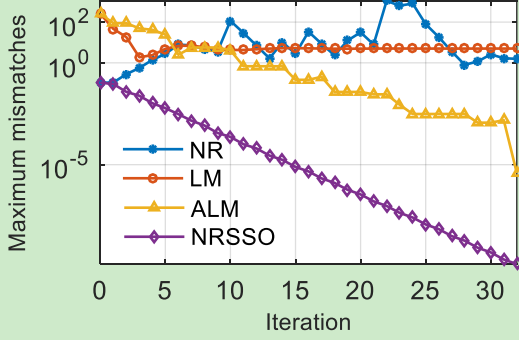


Fig. 6. Maximum mismatches in load flow for 6-bus IMG

The proposed direct NR algorithm is proved to diverge, so the NRSSO method is applied to power load calculation of this IMG. Obviously, there are 2 droop buses, 4 PQ buses and no PV buses in this 6-bus IMG. For each bus, we have 6 power balance equations, so  $F = [\Delta P_1^a, \Delta P_1^b, \Delta P_1^c \dots \Delta P_6^a, \Delta P_6^b, \Delta P_6^c, \Delta Q_1^a, \Delta Q_1^b, \Delta Q_1^c, \dots, \Delta Q_6^a, \Delta Q_6^b, \Delta Q_6^c]^T$ . Take the voltage angle of an arbitrary bus say  $\delta_2^a$  as the reference angle. The unknowns in (16) are expressed in one column vector, i.e.  $X = [\delta_1^a, \delta_2^b, \delta_2^c, \dots, \delta_5^a, \delta_5^b, \delta_5^c, \delta_6^a; U_1^a, U_2^a, U_2^b, U_2^c, \dots, U_5^a, U_5^b, U_5^c, U_6^a; \omega; P_{Droop1}^a, P_{Droop1}^b, Q_{Droop1}^a, Q_{Droop1}^b, P_{Droop6}^a, P_{Droop6}^b, Q_{Droop6}^a, Q_{Droop6}^b]^T$ . Thus, both  $F$  and  $X$  are column vectors with dimension of  $18 \times 1$ . Then an  $18 \times 18$ -dimensional Jacobin matrix  $J$  is composed of the partial derivatives of each element in  $F$  with respect to each element in  $X$  in each iteration. For initialization, the angles of voltage are set as 0; while other unknowns are set as their nominal values. Then the iteration is repeated until  $\|F\|_\infty < \varepsilon$  ( $\varepsilon = 10^{-5}$  p.u.).

To investigate the performance of the proposed method, load flow calculation is performed on this 6-bus system using the LM, ALM, direct NR and NRSSO method. The maximum mismatches in iterations (in p.u.) are shown in Fig. 6. As can be seen from Fig. 6 that for this 6-bus system, when  $\varepsilon = 10^{-5}$  p.u., the direct NR and LM method are divergent, whereas ALM converge after 32 iterations and the proposed NRSSO converge after 15 iterations. The

three-phase node voltages and frequency are illustrated in Table 8. Table 9 shows the OMs  $\mu^{(k)}$  in the  $k$ -th iterations.

**Case 2.** The proposed algorithm is performed on a 25-bus IMG. The single-line diagram and original parameters can be found in [31]. The parameters of droop-controlled DGs integrated are given in Tables 10 (in p.u.,  $S_B = 1\text{MVA}$ ). The ZIP coefficients in load model for all buses and phases are supposed to be the same as the 33-bus IMG.

The proposed direct NR algorithm is proved to diverge, so the NRSSO method is applied to power load calculation of this IMG. Obviously, there are 3 droop buses, 22 PQ buses and no PV buses in this 25-bus IMG. For each bus, we have 6 power balance equations, so  $F = [\Delta P_1^a, \Delta P_1^b, \Delta P_1^c \dots \Delta P_{25}^a, \Delta P_{25}^b, \Delta P_{25}^c, \Delta Q_1^a, \Delta Q_1^b, \Delta Q_1^c, \dots, \Delta Q_{25}^a, \Delta Q_{25}^b, \Delta Q_{25}^c]^T$ . Suppose  $\delta_1^a$  as the reference angle, and  $X = [\delta_i^a, \delta_j^a, \delta_j^b, \delta_j^c; U_i^a, U_j^a, U_j^b, U_j^c; \omega; P_{Droopi}^a, P_{Droopi}^b, Q_{Droopi}^a, Q_{Droopi}^b, i \in \{13, 19, 25\}, j \in \{1, 2, \dots, 12, 14, 15, \dots, 18, 20, 21, \dots, 24\}]$ . Thus, both  $F$  and  $X$  are column vectors with dimension of  $75 \times 1$ . Then a  $75 \times 75$ -dimensional Jacobin matrix  $J$  is composed of the partial derivatives of each element in  $F$  with respect to each element in  $X$  in each iteration. The initialization and the stop criterion are the same as in the 6-bus IMG.

In three-phase unbalanced systems, apart from R/X ratio and feeder loading, the degree of imbalance may influence the convergence of load flow. To investigate the robustness of the NRSSO method, the parameters of the 25-bus IMG are modified and tested. Due to limited space, two cases are given here:

Scenario I. The original system as baseline case;

Scenario II. The loads in Phase A and B increase by 30% and in Phase C increase by 80%; and the line resistance increases by 100%, making a heavier loading condition and

Table 9 OMs  $\mu^{(k)}$  in the  $k$ -th iterations of the 6-bus IMG

$k$	$\mu^{(k)}$	$k$	$\mu^{(k)}$	$k$	$\mu^{(k)}$
1	0.6354	6	0.5133	11	0.5055
2	0.5383	7	0.5012	12	0.5073
3	0.4942	8	0.5085	13	0.5069
4	0.5229	9	0.5036	14	0.5082
5	0.4977	10	0.5070	15	0.5080

Table 10 The parameters of droop-controlled DGs in the 25-bus IMG (p.u.)

Bus No.	Rated capacity	$U_*$	$\omega_*$	$m_p$	$n_Q$
13	0.75	1.05	1.0	0.0040	0.080
19	0.60	1.05	1.0	0.0050	0.080
25	0.75	1.05	1.0	0.0040	0.067

Table 8 Three-phase voltage and frequency of the 6-bus IMG (p.u.)

Bus No.	Phase A	Phase B	Phase C
1	1.0482 $\angle$ 0.000°	1.0482 $\angle$ -120.000°	1.0482 $\angle$ 120.000°
2	1.0332 $\angle$ -0.316°	1.0293 $\angle$ -120.450°	1.0265 $\angle$ 119.659°
3	1.0306 $\angle$ -0.536°	1.0265 $\angle$ -120.672°	1.0288 $\angle$ 119.450°
4	1.0246 $\angle$ -0.500°	1.0184 $\angle$ -120.712°	1.0141 $\angle$ 119.460°
5	1.0260 $\angle$ -0.534°	1.0211 $\angle$ -120.689°	1.0157 $\angle$ 119.473°
6	1.0426 $\angle$ -0.803°	1.0426 $\angle$ -120.803°	1.0426 $\angle$ 119.197°
$\omega$	0.9999		

a higher R/X ratio.

Then the maximum mismatches in iterations (in p.u.) for the two scenarios using NR, LM and ALM method and the proposed NRSSO method are shown in Fig.7. It can be seen from Fig. 7 that when  $\epsilon=10^{-5}$  p.u., the direct NR and LM method are divergent, whereas ALM converge after 81 iterations and the proposed NRSSO converge 21 iterations.

**Case 3.** The algorithm is performed similarly on a 49-bus IMG formed by merging bus 25 in one of the above 25-bus system and bus 1 in another same system. The maximum mismatches in iterations (in p.u.) for the two scenarios by the proposed NRSSO method and NR, LM and ALM method are shown in Fig.8 respectively. Obviously, only the proposed NRSSO converge after 21 iterations.

**Case 4.** The algorithm is performed further on a 73-bus IMG and a 97-bus IMG formed by three and four of the above 25-bus systems in the similar way, respectively. The maximum mismatches in iterations (in p.u.) for the two IMGs using the proposed NRSSO method and the standard NR, LM and ALM method are shown in Fig.9 and Fig.10 respectively. Similar to Case 3, only the proposed NRSSO converge after 21 iterations.

The results in Fig. 6 to Fig. 10 verify the effectiveness and robustness of the NRSSO method. While all other methods fail, NRSSO is able to converge steadily. The comparison of the mismatch curves by NR method and NRSSO show the significance of step size optimization for load flow of three-phase unbalanced IMGs. The OMs help smooth the iterative process and obtain the solution.

Moreover, Table 11 illustrate the computation time of the 6-bus IMG, the 25-bus and 49-bus IMGs in Scenario I, and the 73-bus and 97-bus IMGs. As can be seen the time of the proposed method is less half of ALM method.

From Table 10 and Fig. 6 to Fig.10, the proposed NRSSO method outperforms LM and ALM method on both convergence and computational efficiency.

From the results of all the above balanced and unbalanced cases, it can be seen that the direct NR method has good convergence performance for load flow calculation of three-phase balanced IMGs; whereas for load flow calculation of the three-phase unbalanced IMGs, step size optimization plays a significant role in convergence improvement of NR method.

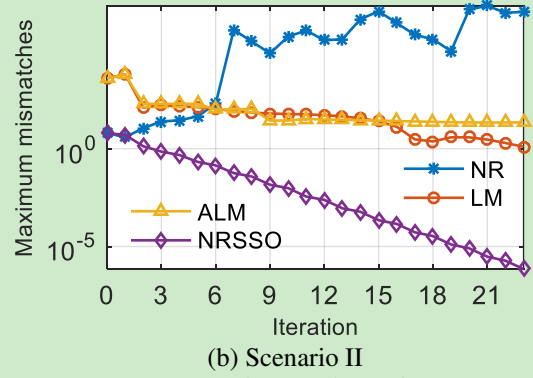
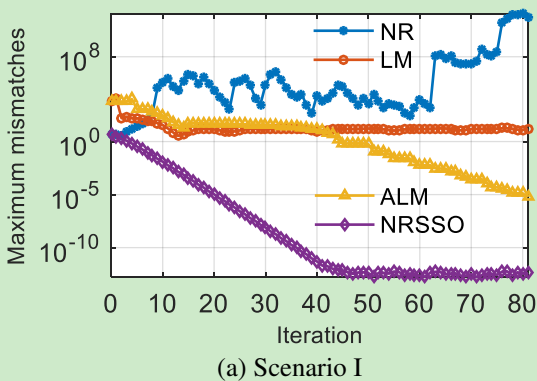


Fig. 7. Maximum mismatches for the 25-bus IMG

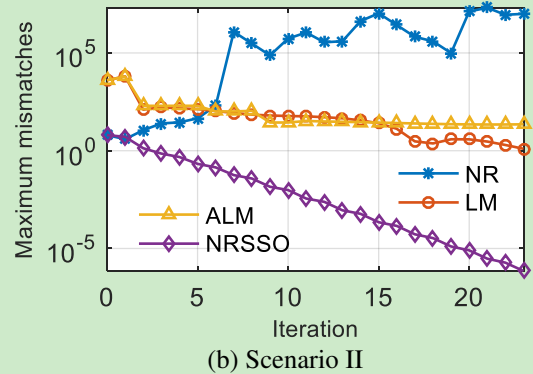
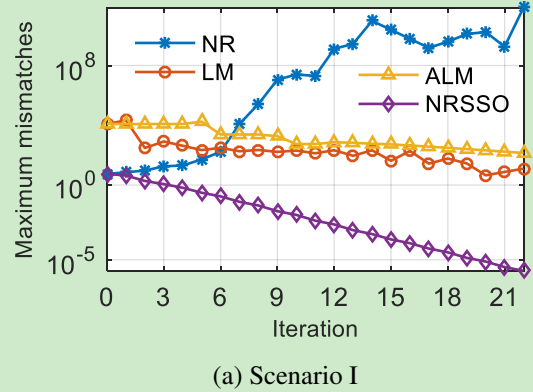


Fig. 8. Maximum mismatches for the 49-bus IMG

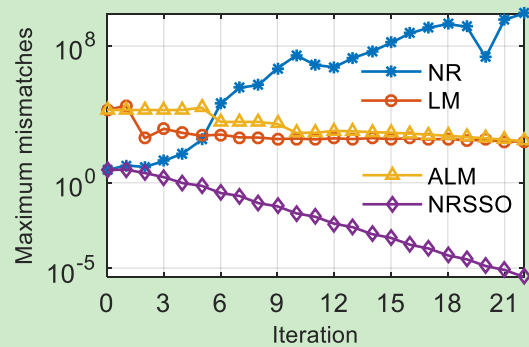


Fig. 9. Maximum mismatches for the 73-bus IMG

Table 11 Computation time (s) of different methods for the IMGs

time	6-bus	25-bus	49-bus	73-bus	97-bus
ALM	0.0212	0.6305	NC	NC	NC
NRSSO	0.0101	0.1164	0.3703	0.8494	1.4533

\*NC means "Not convergent"

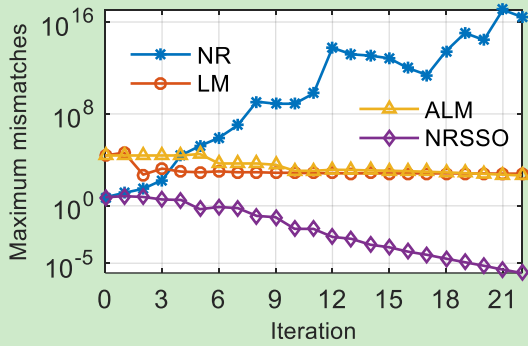


Fig. 10. Maximum mismatches for the 97-bus IMG

## 7. Conclusion

In this work, a load flow algorithm based on direct NR method with step size optimization technique has been proposed for both balanced and unbalanced droop-controlled IMGs. The frequency is treated as an unknown variable and solved together with voltages through the nonlinear load flow equations directly. Thus, the proposed direct NR algorithm has a simple structure. To improve the convergence performance of the algorithm, the step sizes in iterations are optimized by OMs deduced from the whole high-order terms of the Taylor expansion of load flow equations. The algorithm is performed on several balanced and unbalanced IMGs and compared with the LM method and ALM method.

The numerical studies show that:

1) For the balanced droop-controlled IMGs, the proposed direct NR method has good convergence performance and generally don't need step size optimization. It can converge in cases where LM and ALM methods fail. Moreover, it needs less iterations and computation time than LM and ALM methods to achieve the same accuracy.

2) For the unbalanced droop-controlled IMGs, the iteration methods of NR, LM and ALM are faced with challenge of convergence. The proposed direct NR method must work together with step size optimization technique. After optimization, the algorithm, i.e. NRSSO algorithm can converge well whereas in most cases LM and ALM methods fail. Moreover, the computation burden is less than LM and ALM methods.

Over all, the proposed method shows robust and acceptable performance of convergence and efficiency. Therefore, it can be further implemented to probabilistic analysis and optimization problems or be extended to harmonic analysis. Moreover, for a better performance, in cases of adverse initial setpoints, the proposed method can work together with the holomorphic embedding power flow method which is not sensitive to initial setpoints. These points are to be investigated in the future.

## 8. Acknowledgments

This research was supported by the China Scholarship Council (201908615087), National Natural Science Foundation of China (51677151), and Doctoral Start-up Foundation of Xi'an University of Technology.

## 9. References

- [1] Deng, Y., Tao, Y., Chen, G., *et al.*: 'Enhanced power flow control for grid-connected droop-controlled inverters with improved stability', *IEEE Transactions on Industrial Electronics*, 2016, **64**, (7), pp. 5919-5929.
- [2] Guerrero, J. M., Vasquez, J. C., Matas, J., *et al.*: 'Hierarchical control of droop-controlled AC and DC microgrids—a general approach toward standardization', *IEEE Transactions on industrial electronics*, 2010, **58**, (1), pp. 158-172.
- [3] Abdelaziz, M. M. A., Farag, H. E., and El-Saadany, E. F.: 'Optimum droop parameter settings of islanded microgrids with renewable energy resources', *IEEE Transactions on Sustainable Energy*, 2014, **5**, (2), pp. 434-445.
- [4] Abdelaziz, M. M. A., Farag, H. E., and El-Saadany, E. F.: 'Optimum reconfiguration of droop-controlled islanded microgrids', *IEEE Transactions on Power Systems*, 2015, **31**, (3), pp. 2144-2153.
- [5] Amini, M.H., Bahrami, S., Kamyab, F., *et al.*: 'Decomposition methods for distributed optimal power flow: panorama and case studies of the DC model', in Zobaa, A.F., Abdel Aleem, S.H.E., Abdelaziz, A.Y., *et al.*: 'Classical and recent aspects of power system optimization' (Academic Press, USA, 2018, 1<sup>st</sup> edn), pp. 137-155.
- [6] Abdel-Akher, M.: 'Voltage stability analysis of unbalanced distribution systems using backward/forward sweep load-flow analysis method with secant predictor', *IET generation, transmission & distribution*, 2013, **7**, (3), pp. 309-317.
- [7] Alinjak, T., Pavić, I., and Stojkov, M.: 'Improvement of backward/forward sweep power flow method by using modified breadth-first search strategy', *IET Generation, Transmission & Distribution*, 2017, **11**, (1), pp. 102-109.
- [8] Bompard, E., Carpaneto, E., Chicco, G., *et al.*: 'Convergence of the backward/forward sweep method for the load-flow analysis of radial distribution systems', *International journal of electrical power & energy systems*, 2000, **22**, (7), pp. 521-530.
- [9] Díaz, G., Gómez-Aleixandre, J., and Coto, J.: 'Direct backward/forward sweep algorithm for solving load power flows in AC droop-regulated microgrids', *IEEE Transactions on Smart Grid*, 2015, **7**, (5), pp. 2208-2217.
- [10] Nassar, M. E. and Salama, M. M. A.: 'A novel branch-based power flow algorithm for islanded AC microgrids', *Electric Power Systems Research*, 2017, **146**, pp. 51-62.
- [11] Kryonidis, G.C., Kontis, E.O., Chrysochos, A.I., *et al.*: 'Power flow of islanded AC microgrids: revisited', *IEEE Transactions on Smart Grid*, 2018, **9**, (4), pp. 3903-3905.
- [12] Mumtaz, F., Syed, M., Al Hosani, M., *et al.*: 'A novel approach to solve power flow for islanded microgrids using modified Newton Raphson with droop control of DG', *IEEE Transactions on Sustainable Energy*, 2015, **7**, (2), pp. 493-503.
- [13] Nazari, A. A., Keypour, R., Beiranvand, M., *et al.*: 'A decoupled extended power flow analysis based on Newton-Raphson method for islanded microgrids', *International Journal of Electrical Power & Energy Systems*, 2020, **117**, p. 105705.
- [14] Eajal, A., Abdelwahed, M. A., El-Saadany, E., *et al.*: 'A unified approach to the power flow analysis of AC/DC hybrid microgrids', *IEEE Transactions on Sustainable Energy*, 2016, **7**, (3), pp. 1145-1158.
- [15] Amini, K. and Rostami, F.: 'Three-steps modified levenberg-marquardt method with a new line search for systems of nonlinear equations', *Journal of Computational and Applied Mathematics*, 2016, **300**, pp. 30-42.
- [16] Ma, C. and Jiang, L.: 'Some research on levenberg-marquardt method for the nonlinear equations', *Applied mathematics and Computation*, 2007, **184**, (2), pp. 1032-1040.
- [17] Li, C., Chaudhary, S. K., Savaghebi, M., *et al.*: 'Power flow analysis for low-voltage AC and DC microgrids considering droop control and virtual impedance', *IEEE Transactions on Smart Grid*, 2016, **8**, (6), pp. 2754-2764.
- [18] Wang, H., Yan, Z., Xu, X., *et al.*: 'Evaluating influence of variable renewable energy generation on islanded microgrid power flow', *IEEE Access*, 2018, **6**, pp. 71339-71349.
- [19] Wang, H., Yan, Z., Xu, X., *et al.*: 'Probabilistic power flow analysis of microgrid with renewable energy', *International Journal of Electrical Power & Energy Systems*, 2020, **114**, p. 105393.
- [20] Abdelaziz, M. M. A., Farag, H. E., El-Saadany, E. F., *et al.*: 'A novel and generalized three-phase power flow algorithm for islanded microgrids using a Newton trust region method', *IEEE Transactions on Power Systems*, 2012, **28**, (1), pp. 190-201.

- [21] Esmaeli, A., Abedini, M., and Moradi, M. H.: 'A novel power flow analysis in an islanded renewable microgrid', *Renewable energy*, 2016, **96**, pp. 914-927.
- [22] Baghaee, H. R., Mirsalim, M., Gharehpetian, G. B., *et al.*: 'Three-phase AC/DC power-flow for balanced/unbalanced microgrids including wind/solar, droop-controlled and electronically-coupled distributed energy resources using radial basis function neural networks', *IET Power Electronics*, 2017, **10**, (3), pp. 313-328.
- [23] Wang, X., Shahidehpour, M., Jiang, C., *et al.*: 'Three-phase distribution power flow calculation for loop-based microgrids', *IEEE Transactions on Power Systems*, 2017, **33**, (4), pp. 3955-3967.
- [24] Fang, X., Li, F., Wei, Y., *et al.*: 'Reactive power planning under high penetration of wind energy using Benders decomposition ', *IET Generation, Transmission & Distribution*, 2015, **9**, (14), pp. 1835-1844.
- [25] Iwamoto, S. and Tamura, Y.: 'A load flow calculation method for ill-conditioned power systems', *IEEE Transactions on Power Apparatus and Systems*, 1981, (4), pp. 1736-1743.
- [26] Braz, L. M., Castro, C. A., and Murati, C.: 'A critical evaluation of step size optimization based load flow methods', *IEEE Transactions on Power Systems*, 2000, **15**, (1), pp. 202-207.
- [27] Tate, J. E. and Overbye, T. J.: 'A comparison of the optimal multiplier in polar and rectangular coordinates', *IEEE Transactions on Power Systems*, 2005, **20**, (4), pp. 1667-1674.
- [28] Baran, M. E. and Wu, F. F.: 'Network reconfiguration in distribution systems for loss reduction and load balancing', *IEEE Power Engineering Review*, 1989, **9**, (4), pp. 101-102.
- [29] Das, D.: 'Optimal placement of capacitors in radial distribution system using a fuzzy-GA method', *International Journal of Electrical Power & Energy Systems*, 2008, **30**, (6-7), pp. 361-367.
- [30] Khodr, H., Olsina, F., De Oliveira-De Jesus, P., *et al.*: 'Maximum savings approach for location and sizing of capacitors in distribution systems', *Electric Power Systems Research*, 2008, **78**, (7), pp. 1192-1203.
- [31] Raju, G. V. and Bijwe, P.: 'Efficient reconfiguration of balanced and unbalanced distribution systems for loss minimisation', *IET Generation, Transmission & Distribution*, 2008, **2**, (1), pp. 7-12.

## 10. Appendices

**Table 9** The parameters of lines and loads in the 6-bus IMG

Node <i>i</i>	Node <i>j</i>	Length/m	Active power/kW			Reactive power/kVar		
			A	B	C	A	B	C
1	2	128.0	28	22	30	27	54	39
2	3	73.2	24	20	36	30	54	39
3	4	73.2	16	12	24	18	48	36
3	5	73.2	24	20	36	30	54	39
3	6	73.2	20	14	24	21	42	33